TECHNICAL REVIEW

No. 1 – 2013

Noise Test of Revised Notched Nozzle Using a Jet Engine

Heat Conduction Correction in Reciprocity Calibration of Laboratory Standard Microphones

www.bksv.com

Brüel & Kjær

Previously issued numbers of Brüel & Kjær Technical Review

1 – 2012 High-resolution Fly-over Beamforming
Clustering Approaches to Automatic Modal Parameter Estimation

1 – 2011 Performance Investigation of the Dual-Layer Array (DLA) at Low Frequencies
Calculating the Sound Field in an Acoustic Intensity Probe Calibrator – A Practical Utilisation of Boundary Element Modelling
Multi-field Microphone – When the Sound Field is Unknown

1 – 2010 Time Selective Response Measurements – Good Practices and Uncertainty
Measurement of Absorption Coefficient, Radiated and Absorbed Intensity on the Panels of a Vehicle Cabin using a Dual Layer Array with Integrated Position Measurement
ISO 16063 – 11: Uncertainties in Primary Vibration Calibration by Laser Interferometry – Reference Planes and Transverse Motion

1 – 2009 Use of Volume Velocity Sound Sources in the Measurement of Acoustic Frequency Response Functions
Turnkey Free-field Reciprocity System for Primary Microphone Calibration

1 – 2008 ISO 16063–11: Primary Vibration Calibration by Laser Interferometry: Evaluation of Sine Approximation Realised by FFT
Infrasound Calibration of Measurement Microphones
Improved Temperature Specifications for Transducers with Built-in Electronics

1 – 2007 Measurement of Normal Incidence Transmission Loss and Other Acoustical Properties of Materials Placed in a Standing Wave Tube

1 – 2006 Dyn-X Technology: 160 dB in One Input Range
Order Tracking in Vibro-acoustic Measurements: A Novel Approach Eliminating the Tacho Probe
Comparison of Acoustic Holography Methods for Surface Velocity Determination on a Vibrating Panel

1 – 2005 Acoustical Solutions in the Design of a Measurement Microphone for Surface Mounting
Combined NAH and Beamforming Using the Same Array
Patch Near-field Acoustical Holography Using a New Statistically Optimal Method

1 – 2004 Beamforming

1 – 2002 A New Design Principle for Triaxial Piezoelectric Accelerometers
Use of FE Models in the Optimisation of Accelerometer Designs
System for Measurement of Microphone Distortion and Linearity from Medium to Very High Levels

(Continued on cover page 3)

Technical Review

No. 1 – 2013

Contents

Editor: Harry K. Zaveri

Noise Test of Revised Notched Nozzle Using a Jet Engine

Tatsuya Ishii[*], *Nozomi Tanaka*[†], *Tsutomu Oishi*[‡] *and Yutaka Ishii*[**]

Abstract

This paper describes engine noise tests conducted in an outdoor environment using a revised notched nozzle. A notch is a small dent formed at the nozzle edge that penetrates into the primary jet. The notched nozzle is expected to improve the acoustic performance with less deterioration in aerodynamic performance relative to that of a conventional nozzle. The slight penetration of the notch causes small disturbances immediately after the nozzle, driving the subsequent mixing process in the shear layer. This mixing process helps suppress both large-scale vortices in the far downstream region and excessive shear stress near the nozzle.

The authors have researched and developed various notched nozzles. Previous engine tests using a 6-notched nozzle showed that the notch itself caused additional noise by increasing the sound pressure level at higher frequencies. To counter this problem, a revised 18-notched nozzle was developed through computational and experimental studies. The authors' previous paper [Ishii, et al.; ASME Paper GT2012-69507, 2012] showed that this nozzle increased the noise reduction toward the side direction of the nozzle under hot-jet conditions. However, there remain some unsolved issues. One issue is the scale of the nozzle. Another issue is the test conditions, such as the different effective cross-sectional areas.

* Aviation Program Group, Japan Aerospace Exploration Agency, 7-44-1 Jindaijihigashi-machi, Tokyo, Japan, E-mail: ishii.tatsuya@jaxa.jp

† Aero-Engine & Space Operations, IHI Corporation, 229 Tonogaya Nishitama-gun, Tokyo, Japan, E-mail: Nozomi_tanaka@ihi.co.jp

‡ Aero-Engine & Space Operations, IHI Corporation, 229 Tonogaya Nishitama-gun, Tokyo, Japan, E-mail: Tsutomu_ooishi@ihi.co.jp

** Brüel & Kjær Japan, 2-6 Kanda-tsukasamachi, Tokyo, Japan, E-mail: Yutaka.Ishii@bksv.com

In this light, a larger-scale nozzle with a diameter five times larger than that in the hot-jet model was prepared so as to adjust the nozzle aerodynamic performance. Noise tests of this nozzle were carried out using a turbojet engine together with far-field and phased array microphones, and the revised notched nozzle was found to show improved noise reduction performance compared to the previous design.

Résumé

Le présent document décrit des essais de bruit de moteur réalisés en extérieur et pour lesquels a été utilisée une tuyère qui a été crantée sur l'extrémité en contact avec le jet primaire. Cette modification est censée améliorer les performances acoustiques en atténuant la dégradation des caractéristiques aérodynamiques. La légère pénétration des crans cause de petites turbulences en sortie immédiate de la tuyère, entraînant le processus de mélange subséquent au niveau de la couche de cisaillement. Ce processus de mélange aide à supprimer tant les fortes turbulences dans la région éloignée en aval du flux que le cisaillement excessif près de la tuyère.

Les auteurs ont mis au point différents modèles. Des essais précédents, réalisés avec un modèle à six crans avaient montré que les crans étaient en soi cause de bruit supplémentaire en augmentant le niveau de pression acoustique aux hautes fréquences. Ce problème a été corrigé via une approche expérimentale et informatique par la mise au point d'un modèle à dix-huit crans. Dans un document précédent [Ishii, et al.; ASME Paper GT2012-69507, 2012], les auteurs avaient montré que ce modèle permettait une réduction du bruit dans la direction latérale dans des conditions de jet d'air chaud. Certaines questions restaient cependant non résolues, relatives notamment à la taille de la tuyère, ou aux conditions d'essais, par exemple la surface effective des différentes sections transversales.

C'est pourquoi un modèle beaucoup plus grand a été mis au point, au diamètre cinq fois plus grand que celui du modèle à jet chaud, afin de travailler sur l'aérodynamisme de la tuyère. Les essais acoustiques ont été conduits sur un turboréacteur au moyen d'une antenne microphonique à commande de phase et de microphones en champ lointain. Comparée au modèle précédent, la tuyère ainsi modifiée s'est avérée plus performante pour la réduction du bruit.

Zusammenfassung

Dieser Artikel beschreibt Geräuschmessungen an Triebwerken im Freien, die mit einer überarbeiteten gekerbten Düse durchgeführt wurden. Bei den Kerben handelt es sich um kleine Ausbuchtungen an der Düsenkante, die in den Hauptstrahl gerichtet sind. Man erwartet, dass die gekerbte Düse die akustischen Eigenschaften verbessert, indem die Aerodynamik weniger gestört wird als mit einer herkömmlichen Düse. Das geringfügige Eindringen der Kerbe verursacht kleine Störungen unmittelbar hinter der Düse und fördert den nachfolgenden Mischprozess in der Scherschicht. Dieser Mischprozess hilft großräumige Wirbel im weiter stromabwärts gelegenen Bereich sowie übermäßige Schubspannungen nahe der Düse zu unterdrücken.

Die Autoren haben unterschiedliche gekerbte Düsen untersucht und entwickelt. Frühere Triebwerksmessungen mit einer sechsfach gekerbten Düse hatten gezeigt, dass die Kerbe selbst zusätzliche Geräusche erzeugt und den Schalldruckpegel bei höheren Frequenzen erhöht. Um diesem Problem abzuhelfen, wurde anhand rechnerischer und experimenteller Untersuchungen eine überarbeitete Düse mit 18 Kerben entwickelt. Der frühere Artikel der Autoren [Ishii, et al.; ASME Paper GT2012-69507, 2012] zeigte, dass diese Düse die Geräuschreduzierung in seitlicher Richtung der Düse unter Heißstrahl-Bedingungen verbesserte. Es verbleiben jedoch einige ungelöste Probleme. Eines davon ist das Größenverhältnis der Düse. Ein anderes sind die Testbedingungen, unter anderem die unterschiedlichen effektiven Querschnittsflächen.

Deshalb wurde eine größere Düse mit dem fünffachen Durchmesser des Heißstrahl-Modells vorbereitet, um die aerodynamischen Eigenschaften der Düse abzustimmen. An einem Turbinen-Luftstrahltriebwerk mit dieser Düse wurden Geräuschmessungen mit Fernfeld- und phasengesteuerten Array-Mikrofonen ausgeführt und festgestellt, dass die überarbeitete gekerbte Düse im Vergleich zur früheren Konstruktion eine bessere Geräuschunterdrückung aufwies.

Introduction

Notched Nozzle

Jet mixing noise produced during aircraft takeoff is of great annoyance; this noise should be reduced in order to improve the noise margin of jet aircraft. Jet mixing noise can basically be reduced by two approaches [1]. One is to adopt a large-bypass-ratio engine that has low mean exhaust velocity that in turn leads to low radiated acoustic power. Another is to attach or redesign a mixer at the end section of the engine.

Many studies have attempted to develop a suitable mixer [2, 3]. In recent times, Chevron nozzles, which have triangular serrations at the nozzle end with some degrees of inclination, have been successfully employed. Studies have investigated the reduction in subsonic and supersonic jet noise using Chevron-type nozzles [4-6]. One of the remarkable differences between this shallower angled serration and the conventional lobed geometry depends upon the extent of the mixing process. Fast mixing, as seen in conventional mixers, between the core flow and the secondary flow accompanies additional noise that degrades noise benefit in the side direction. The slightly inclined serration is designed to control the mixing process within the shear layer behind the nozzle. The microjet concept also ensures a suitable penetration angle and mass-flow rate in order to appropriately regulate the shear stress [7]. This mixing concept is expected to solve issues related to additional noise increase and thrust loss.

A recent international consensus on the trade-off between noise stringency and carbon dioxide emissions has meant that mixers should achieve a noise benefit with only a small thrust penalty. In this light, one of the authors proposed the use of notches as a new type of mixer [8]. Figure 1 shows a schematic view of a notch. A notch is a tiny dent that is formed at the nozzle end. One of its sides penetrates the core flow and the other forms a gutter. The interval between adjacent notches

Fig. 1. Schematic view of notched nozzles

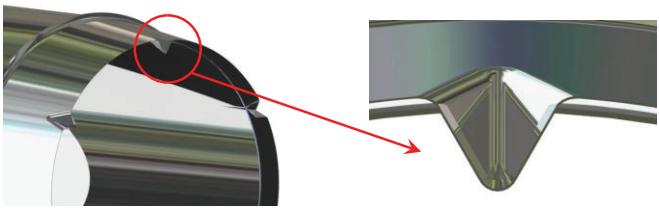

is much larger than the width of a notch, which differentiates a notched nozzle from a lobe-type one. The notched nozzle was proposed and studied under the ECO engine project supported by the New Energy and Industrial Technology Development Organization (NEDO), following which research and development on modifying the notch design has been conducted under a joint study between JAXA and IHI since 2008.

Noise Test with a Jet Engine

In 2008, the first noise test was conducted on a notched nozzle using a jet engine. A 6-notched nozzle was attached to the nozzle end of a turbojet engine. The results showed that this nozzle suppressed broadband noise at middle and lower frequencies; however, additional noise appeared at higher frequencies toward the side direction of the nozzle [9]. A preliminary computation suggested that a larger number of finer notches should be distributed along the nozzle lip [10, 11]. Through a comparison of the turbulent kinetic energy immediately behind the trailing edge of the nozzle, the smaller depth and increased number of notches were determined. A finer 18-notched nozzle was proposed in light of several experimental and design considerations. Scale-model tests of this nozzle were carried out under cold- and hot-jet conditions [12, 13]. The results showed that the noise performance was improved and that the far-field noise level was kept low over wide radiation angles compared to the baseline conical nozzle. Hot-jet results obtained in a previous study [13] suggested that the noise reduction level was slightly increased toward the side direction, which should reduce the perceived noise level (PNL) at a lateral point during takeoff.

However, there remain several unsolved problems. The previous engine test was conducted under rating control, which means that the nozzle pressure ratios (NPRs) differed with the nozzle configuration. In addition, although the revised notched nozzle showed satisfactory noise reduction, the scale-model nozzle with a diameter of 40 or 50 mm was insufficient to evaluate the jet noise under appropriate Reynolds numbers. Aerodynamic data, including the mass flow rate, thrust, and exhaust jet velocity, are also necessary for evaluating the applicability of the notched nozzle to the noise reduction device in aero-engines.

One solution to these problems was to conduct an engine noise test. Thus, the authors planned the noise test of the revised 18-notched nozzle using a larger-scale demonstrator engine. Digitally controlled operation enabled identical NPR conditions with different nozzle configurations. The nozzle diameter of the engine was approximately five times that of the model engine. This paper outlines the

engine noise tests conducted with the baseline and the 18-notched nozzle and primarily discusses the acoustic results.

Experimental Setup

Jet Engine and Test Stand

A jet engine was used to simulate a hot-jet plume in a static field. For this purpose, a turbojet engine with a maximum thrust of up to 8.5 kN was employed [14]. The inlet section of the engine has a two-stage compressor comprising a 17-bladed axial compressor and a centrifugal compressor. A bell-mouth was attached in front of the compressor duct, in which a total pressure rake and a total temperature rake were mounted to estimate the mass flow rate into the engine. A turbulence control device or inflow control device was not installed at the bell-mouth in this test series; therefore, there exists some concern about undesirable noise contamination, especially in the forward radiation.

The exhaust section, comprised of a single-stage turbine and a tail-cone, was connected to a straight tail-pipe. The test nozzle was installed at the end of the tail-pipe. A baseline conical nozzle had an exit diameter of 262 mm. Figure 2 shows a schematic view of the exhaust section, tail-pipe, and nozzle. The primary reason why the tail-pipe was put between the turbine exit and the nozzle is to eliminate the distortion of the upstream flow caused by the turbine and tail-cone. The length

Fig. 2. Schematic view of exhaust section of the engine, tail-pipe, and nozzle

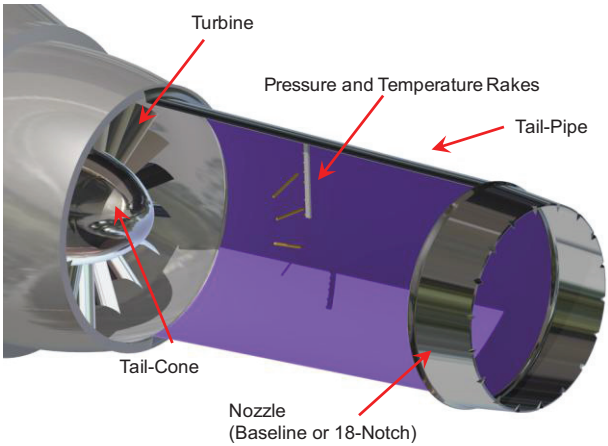

of the tail-pipe was more than 2.5 times the nozzle exit diameter. It is reported that the upstream flow involves disturbances due to the lateral pressure gradient [15, 16]. The generated twist-pair vortices may interfere with the notches. Taking account of the upstream conditions, this noise test focused on not the absolute level of noise but the difference between the radiated noise from the baseline and the notched nozzles. A 6-hole pressure rake and temperature rakes were mounted in the tail-pipe; furthermore, static pressure was monitored at four points at identical axial positions.

This engine and its attachments were placed on a mobile test stand [14, 17]. The mobile test stand includes the thrust-measurement equipment. The stand is set on top of a base stand such that the engine was at a height of 3 m from the ground surface. A fuel tank, auxiliary machinery, and an on-site data transmitter were placed around the base stand. Figure 3 shows the engine noise test layout at JAXA's Noshiro Rocket Test Center. As the test site faces the sea coast, special attention was paid to the treatment of salt and humidity during the night and non-test days.

Fig. 3. Outdoor noise test site and ground microphone stand

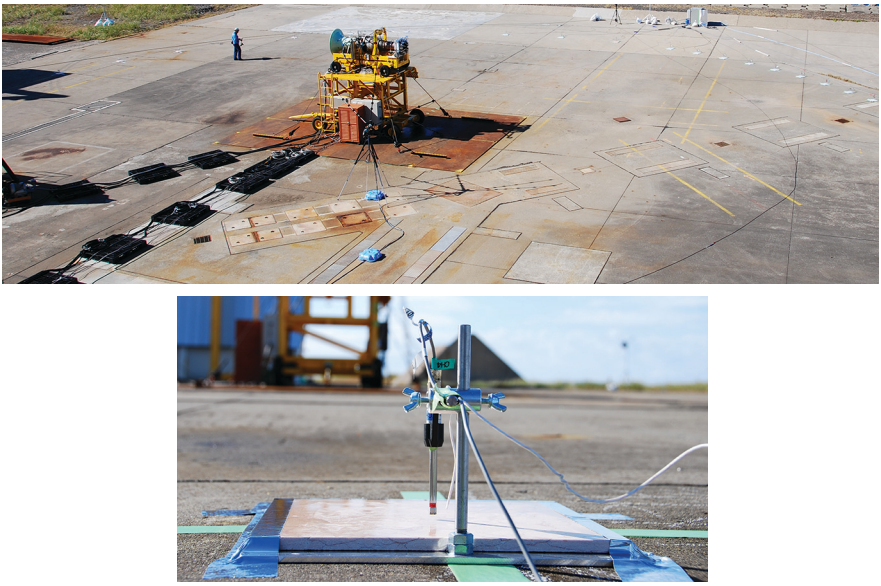

18-Notched Nozzle

The noise reduction performance was compared between the 18-notched nozzle and the baseline nozzle that has a conical geometry. Each nozzle was connected to the straight tail-pipe mentioned above. Both nozzles had almost the same contraction rate toward the nozzle lip but showed different exit geometry. The equivalent cross sections of these nozzles were very similar. The 18-notched nozzle was designed to be slightly larger such that its effective cross-sectional area was identical to that of the baseline nozzle.

The revision of the notch geometry is summarized in Fig. 4, which shows a comparison of the previously tested 6-notched nozzle and the revised 18-notched nozzle. The features of the newly manufactured 18-notched nozzle are as follows:

(1) The number of notches was increased from 6 to 18.
(2) Both notches had approximately similar equilateral-triangle-shaped cross-sectional geometries, and their ratio of longitudinal length to notch depth was almost equal.
(3) The notches were placed at regular intervals along the nozzle lip in both cases.

Fig. 4. Notched nozzles, Left: 6-notched nozzle, Right: Present 18-notched nozzle

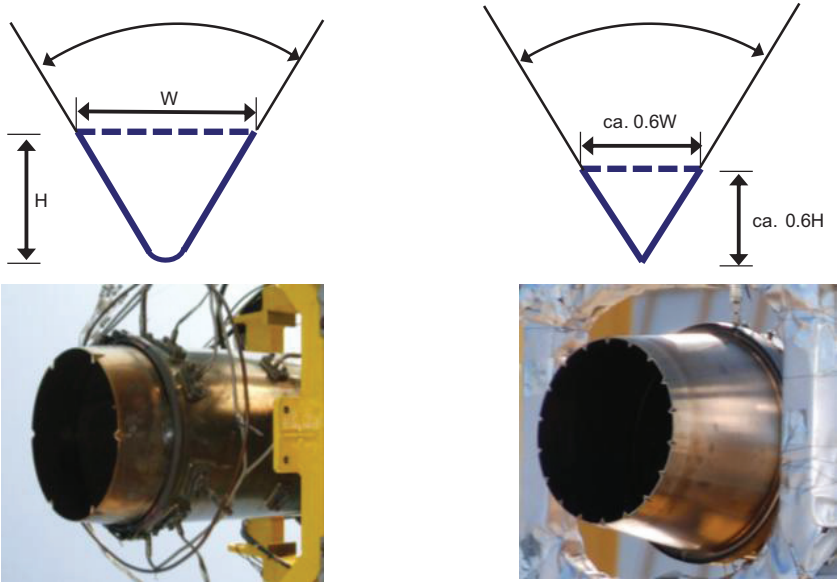

(4) The depth of each notch was decreased from 5% of the nozzle exit diameter to 3%. Accordingly, the width of each notch decreased.
(5) The 18-notched version had a sharp edge at its tip.

Engine Control and Measurement

In this noise test, robust control of the engine state was necessary for realizing identical conditions. An identical NPR was maintained by applying a model-based Kalman filter to the FADEC (Full Authority Digital Electronics Control) unit of the engine [18]. The NPR in this test is defined in terms of the total pressure inside the tail-pipe, $P_{t,6}$, and the atmospheric pressure, P_a, as follows:

$$NPR = \frac{P_{t,6}}{P_a} \tag{1}$$

The exit Mach number is estimated assuming an isentropic process as follows:

$$M_j = \sqrt{\frac{2}{\kappa - 1}\left(NPR^{\frac{\kappa - 1}{\kappa}} - 1 \right)} \tag{2}$$

Here, κ is the ratio of the specific heat of the exhaust gas. It is a function of the air-fuel ratio and static temperature of the exhaust gas.

The engine control unit recorded the time data of other engine parameters such as the rotation speed, exhaust gas temperature (EGT) of the turbine, thrust, total pressure, and total temperature at relevant locations. The thrust measurement system was calibrated in advance using a hydraulic actuator, and it was confirmed to be linear in the thrust range of interest. The atmospheric temperature difference between a point near the engine and the microphone stand was also monitored [19].

The weather data, i.e., atmospheric pressure, temperature, and humidity, together with the wind speed and direction were recorded by a weather station at 60-s intervals. The atmospheric data were time-averaged and referred to for correcting both engine and acoustic data.

Acoustic Measurement Setup

The acoustic measurement was carried out in parallel with engine data recording. This measurement consists of conventional far-field noise measurement using

multiple ground microphones and source localization measurement using a phased-array microphone system.

The 24 ground microphones were deployed along two 18-m-arcs centered at the bell-mouth inlet and nozzle exit. The ground microphone positions are shown in Fig. 5. At each measurement position, a quarter-inch pressure-type microphone (GRAS Type-40BP) was inversely installed by maintaining a quarter-inch interval between the microphone cartridge and a reflective marble plate, as shown in Fig. 3. The acoustic time signal was sent to a signal conditioner (B&K NEXUS) via a pre-amplifier (B&K Type-2669), transformed into 24-bit digital time signals at a sampling rate exceeding 50 kHz, and then stored in data recorders (OROS OR36 and National Instruments NI-DAQ). For each NPR, the acoustic signals of all microphones were simultaneously recorded for 30 s.

Fig. 5. Microphone positions in the far field

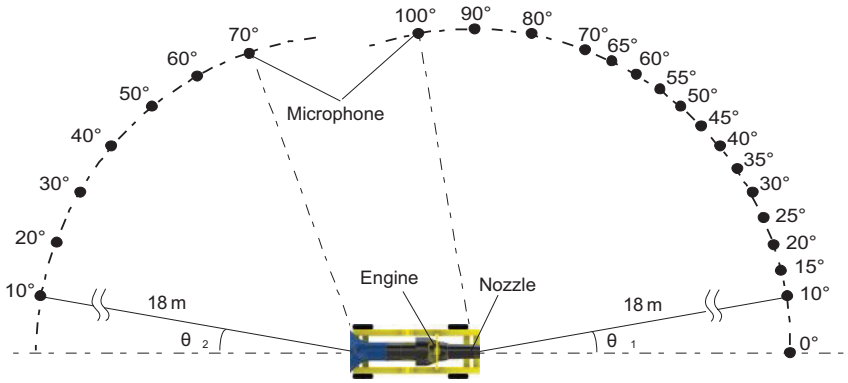

The phased-array microphone (B&K Pentangular Array) was employed to refer to the sound source structure from the lateral angle, which is crucial in evaluating the takeoff noise. The array was then placed parallel to the jet axis [20]. This array comprises 30 microphones on 5 foldable bars and a camera in the center. The available frequency for frequency-domain beamforming ranges from 100 Hz to 5 kHz. The array center was located 3 m downstream of the nozzle and kept at a distance of 5.5 m from the jet axis. The center position of the array was at 2 m from the ground, and the array was tilted so that the focal point was on the jet center line. Figure 6 shows the layout around the engine nozzle. Delay-and-sum beamforming is combined with a de-convolution algorithm in this system [21].

Fig. 6. Layout around engine test stand

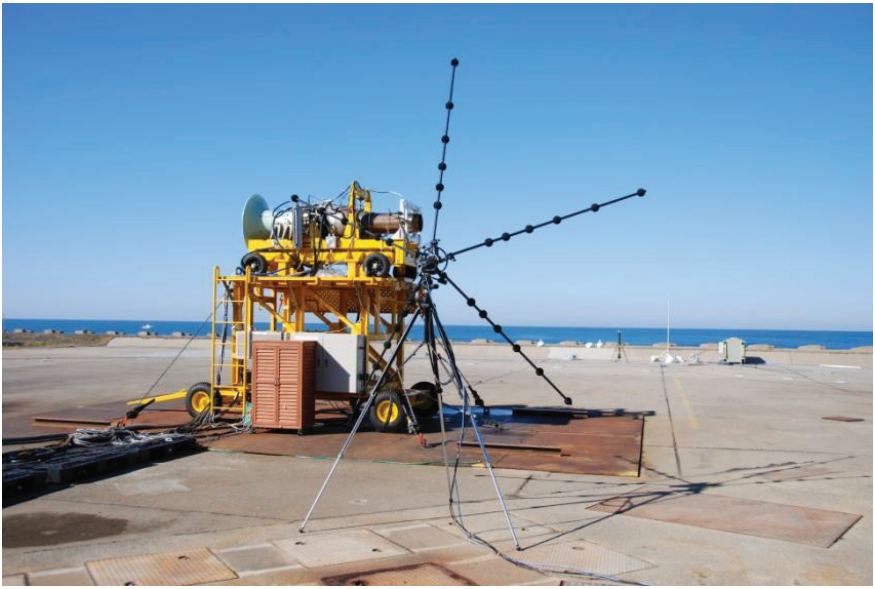

Data Analysis and Test Conditions

Acoustic signals recorded in the test were post-processed and transformed into the average frequency domain forms. The spectra were corrected with regard to the air absorption and ground reflection. A tone-elimination was added to avoid the overestimation due to non-jet mixing noise. The solid line in Fig. 7 shows a representative narrow-band response that was obtained at 55° from the jet axis. Turbo-machinery tones around 5000 Hz and their harmonics are predominant in this response. In addition, scattered turbine noise appears at some rear angles [22]. The predominant component is a tone at around 300 Hz. This omnidirectional anomalous tone in the far-field appears in both the baseline and the 18-notched nozzles. One explanation of this phenomenon is flow instability immediately after the tail-cone. This undesirable tone is also eliminated in the post-processing. The dotted line in Fig. 7 shows the correction with tone-elimination treatment.

Table 1 lists the tested NPRs and the corresponding engine ratings. These values were determined by both the scale-model test cases. At least two operations were implemented for each NPR condition. The repeatability among identical NPRs was sufficient for evaluating the jet mixing noise.

Fig. 7. Example of post-processing

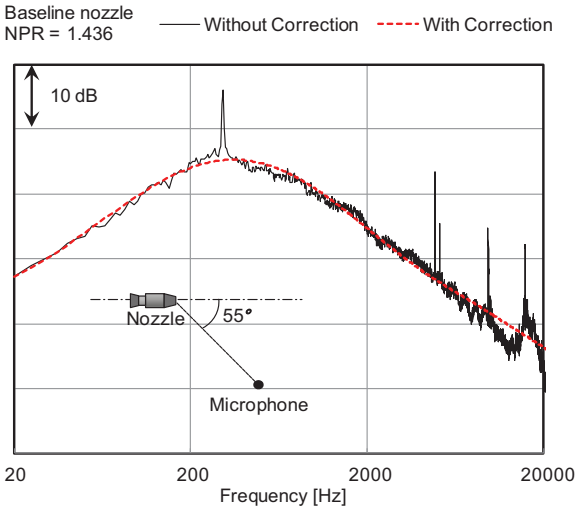

Table 1. Nozzle pressure ratios

NPR	1.377	1.436	1.500	1.536
Rating (%)	75	80	82.5	85

Results and Discussion

Noise Reduction by 18-Notched Nozzle

(1) Reduction in jet mixing noise

Figure 8 shows a comparison between the far-field frequency responses of the baseline nozzle and the 18-notched nozzle under an NPR of 1.536. The spectra were tone-eliminated with air-absorption correction and expressed with regard to the Strouhal number based on the exhaust velocity. The figure shows three representative radiation angles: 30°, 60°, and 90° from the jet. In the 18-notched nozzle, the low-frequency peak (St: ~0.2) at the downstream and the high-frequency broadband noise at the side angle are suppressed by as much as 1.5 dB compared to that in the baseline nozzle. The far-field noise reduction was explained by the mixing enhancement due to the notches and the subsequent attenuated shear stress at the downstream of the nozzle. Mixing enhancement

generally accompanies the additional high-frequency noise sources. The previous notch design suffered from the additional higher-frequency noise that dominated the total acoustic power, especially at side angles [9]. The 18-notched nozzle well suppressed the additional noise, as observed at high frequencies.

Fig. 8. Frequency responses of the baseline and 18-notched nozzles (NPR = 1.536)

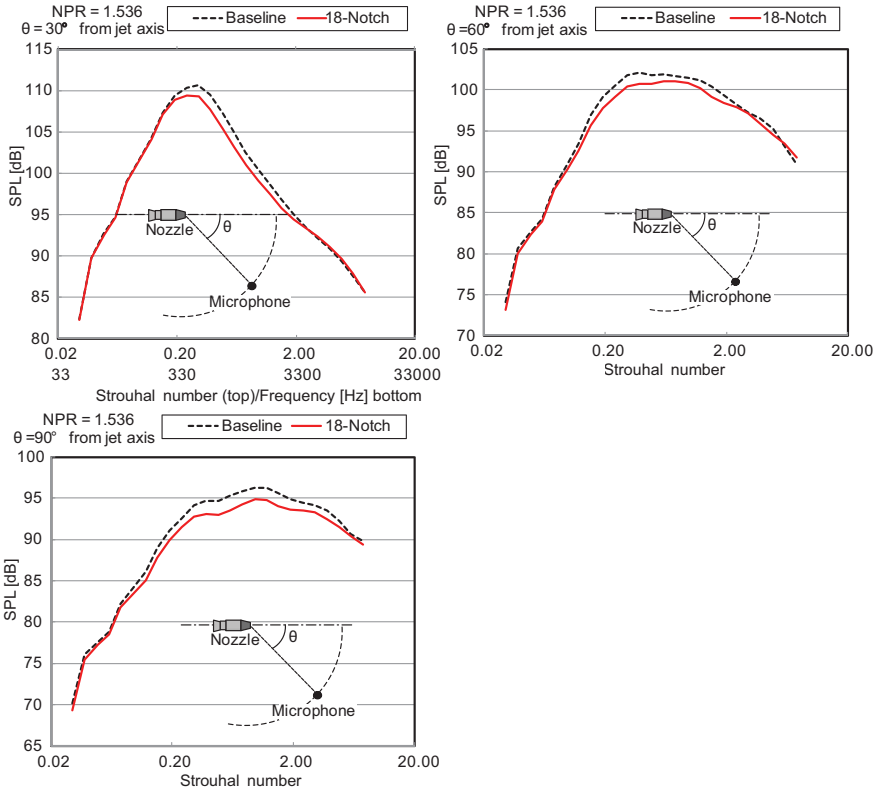

To overview this noise reduction property by the 18-notched nozzle, the noise directivities are plotted in Fig. 9. The overall sound pressure levels were suppressed at almost all radiation angles. This tendency differed from that of the 6-notched nozzle, which increased the noise level at more than 45° [12]. Similar directivities were observed at Strouhal numbers of 0.21 and 1.1, which are around

Fig. 9. Directivity patterns of overall case and Strouhal numbers of 0.21 and 1.1 (NPR = 1.536)

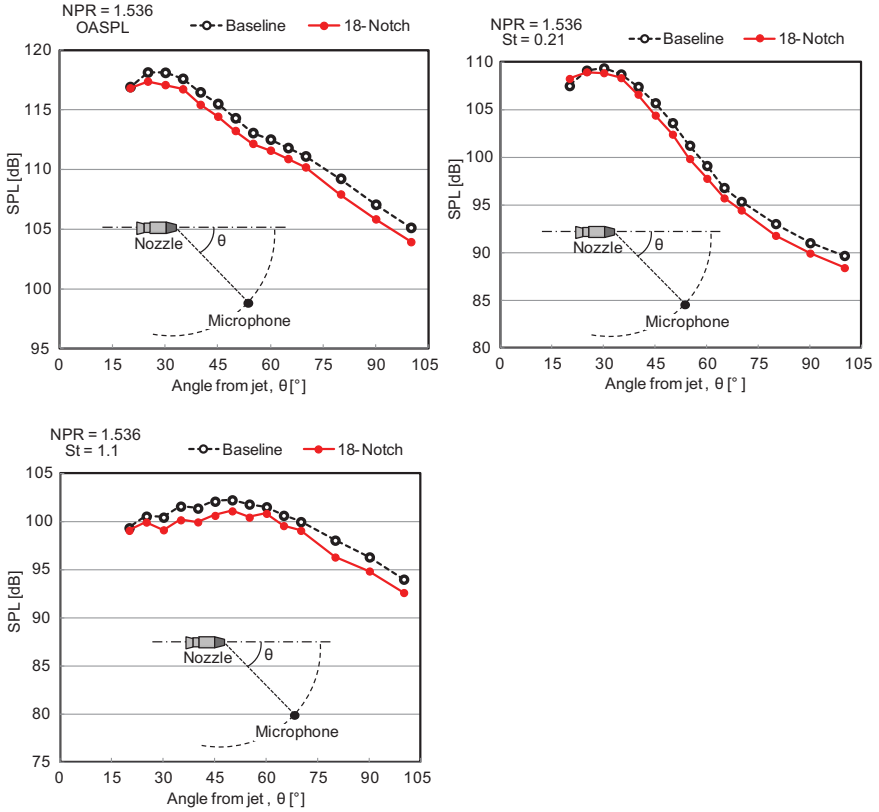

the broadband peak. The noise reduction level increases as the radiation angle approaches the side direction, which coincides with the hot-jet scale-model results [13].

The radiated acoustic power levels were estimated based on the distribution of the far-field sound pressure levels:

$$I_i = \int I_{(i,k)} ds_k \tag{3}$$

$$I_{OA} = \sum_i I_i \tag{4}$$

Here, $I_{(i,k)}$ is the acoustic power per unit area [w/m^2] of the i-th frequency band and k-th element. I_i and I_{OA} are the radiated power of the i-th band and overall power, respectively.

Figure 10 shows a plot of the acoustic power levels of the baseline nozzle and the 18-notched nozzle under NPRs of 1.436 and 1.536. The distribution of the radiated power versus the Strouhal number clearly shows the similarity in the characteristics, with a common peak at a Strouhal number of around 0.25 and reduced radiated power above the peak frequency. Figure 11 shows the dependency of the acoustic power on the Mach number. The acoustic power of the baseline notched nozzle also agrees with the power law, but the radiated acoustic power is less than that of the baseline nozzle. The reduction in the acoustic power increases as the Mach number decreases.

Fig. 10. Frequency responses of radiated acoustic power (NPR = 1.436 and 1.536)

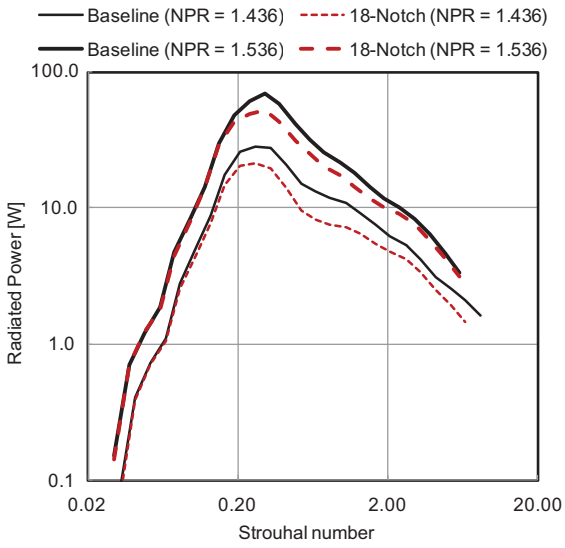

Fig. 11. Dependency of radiated acoustic power on jet Mach number

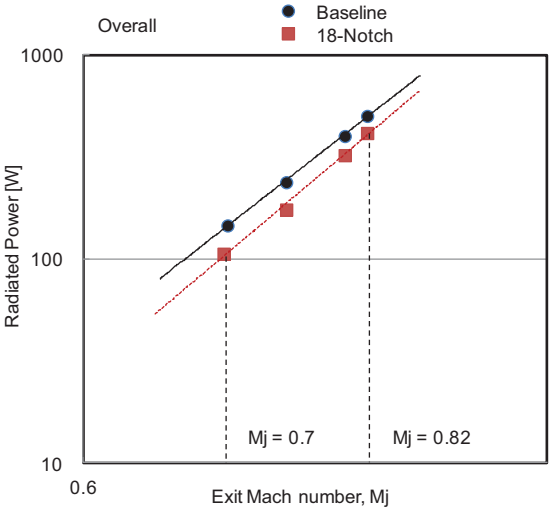

(2) Thrust measurement

According to the thrust measurement, both baseline and 18-notched nozzles showed thrust levels within 1%. The fact that the thrust and exhaust jet velocity were kept almost equal in the present test suggests that the noise data were obtained under satisfactory conditions. Referring to the thrust influence by tabs [15], it was found that a more precise comparison was necessary for evaluating the aerodynamic performance.

The lack of accuracy in evaluating the very small thrust difference arose from the environmental conditions and test techniques. The outdoor environment involves sudden cross-wind, turbulence into the engine, and so on. As for the engine test techniques, NPR control succeeded in maintaining the total pressure in the tail-pipe and nozzle design made the effective cross-sectional area almost identical, enabling reasonably equal thrust and mass flow rates with different nozzle geometries. However, it was also difficult to simultaneously regulate both the thrust and the mass flow rate to satisfactorily evaluate the thrust loss under the present engine control and outdoor test techniques.

(3) Sound source analysis

Figure 12 shows the result of sound source analysis of the baseline nozzle and 18-notched nozzle under NPR of 1.436 as obtained by the phased-array microphone. The source maps in the 400-Hz band are shown at the top of the figure. The sound source in each map is plotted in the level between 92 dB to 102 dB. The sound source stretches beyond 4 or 5 times the nozzle diameter. This fact implies that the low-frequency noise sources are distributed even in the far downstream region.

Fig. 12. Examples of source localization (NPR = 1.436). Figures on the top show sound sources in the 400-Hz band (Strouhal number of 0.26) and those on the bottom, in the 3150-Hz band (Strouhal number of 2.08). Figures on the left are obtained by the baseline nozzle and those on the right, by the 18-notched nozzle

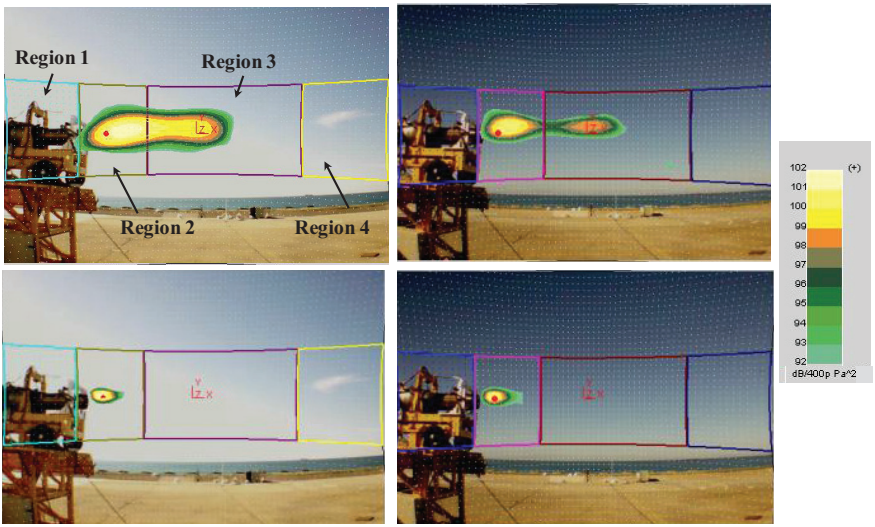

To evaluate the noise benefit of the notch quantitatively, the data on the source maps were transformed into the total power levels. Each source level at each analytical grid was summed in the region concerned. Four regions were selected, as shown in Fig. 12. Region 1 is upstream of the nozzle and is expected to have very little influence as a noise source. Region 2, which is between one to five times the nozzle diameter, is expected to be a strong noise source including both low- and higher-frequency sources. Region 3 neighbors Region 2 and stretches until 20 times the nozzle diameter. This region contains part of lower-frequency noise sources. Region 4 is located far away from the nozzle. Figure 13 summarizes

the rate of the summed acoustic power of each region, namely, the contribution of source strength. The contribution is plotted for each frequency band. The maximum frequency was 1600 Hz considering the accuracy of the data analysis in Regions 1, 3, and 4. The contribution of the sound source near the nozzle (Region 2) increases as the frequency increases. In contrast, that of the sound source in the downstream region (Region 3) decreases as the frequency increases. This result explains that the noise sources at lower frequency tend to be located downstream of the nozzle whereas those at higher frequency are located near the nozzle. This trend of sound source position agrees with the conventional explanation of jet noise source position.

Fig. 13. Contribution of power levels accumulated at each region

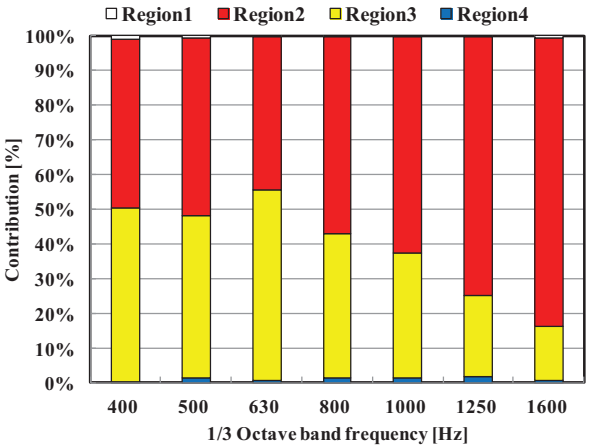

These source maps also support noise reduction by the notch. Comparing the top figures of Fig. 12, it is apparent that the notch slashes the strength and size of the 400-Hz band sound source, which is observed in both Regions 2 and 3. In contrast, the 3150-Hz band sources, shown in the bottom of Fig. 12, are distributed near the nozzle (Region 2), and the noise reduction level appears to be small. Figure 14 shows the reduction of source strength by the 18-notched nozzle in Regions 2 and 3. The summed acoustic power in each region was compared with and without the notch. The power reduction in Region 2 is at most 1 dB, whereas that in Region 3 is no less than 2 dB. These results confirmed that the revised 18-notched nozzle weakens the sound sources over a wide frequency range in the far downstream region.

Fig. 14. Reduction in sound source strength by 18-notched nozzle

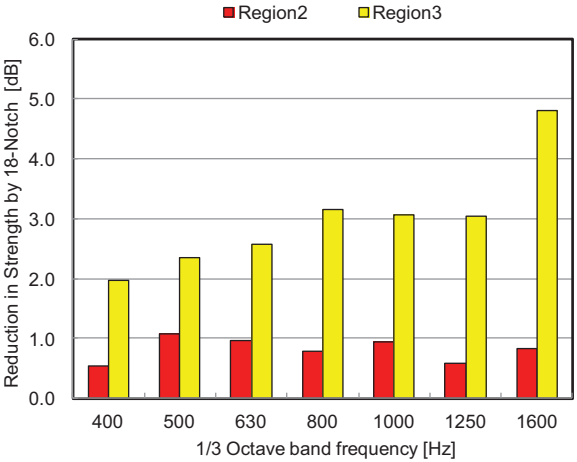

Improvement in Noise Reduction

(1) Comparison of radiated acoustic power

Figure 15 shows a comparison of the radiated acoustic power obtained from the corrected frequency responses of the 6-notched nozzle, 18-notched nozzle, and baseline nozzle at an overall level and at the 400- and 3150-Hz bands. The baseline nozzle here is that applied to the previous test, and its detailed flow condition differs from that of the baseline nozzle in the present test. The overall sound power versus the Mach number clearly shows that the 18-notched nozzle is superior in reducing the radiated power. The velocity dependency also differs depending on the notch configuration. The previous 6-notched nozzle tends to reduce the acoustic power as the Mach number increases. In comparison, the mitigation of the acoustic power by the 18-notched nozzle shows less dependency on the Mach number.

The acoustic power at the representative frequencies shows clearer differences between these notched nozzles. The 18-notched nozzle effectively reduces the acoustic power around the broadband peak, in this case, the 400-Hz band, at lower speeds. On the other hand, the 6-notched nozzle is effective at high subsonic ranges, but its margin to the baseline is limited. At the 3150-Hz band, the acoustic power of the 6-notched nozzle becomes greater than that of the baseline nozzle, which causes inferior acoustic performance.

Fig. 15. Radiated acoustic power levels among the baseline (previous test), 6-notched nozzle (previous test), and 18-notched nozzle

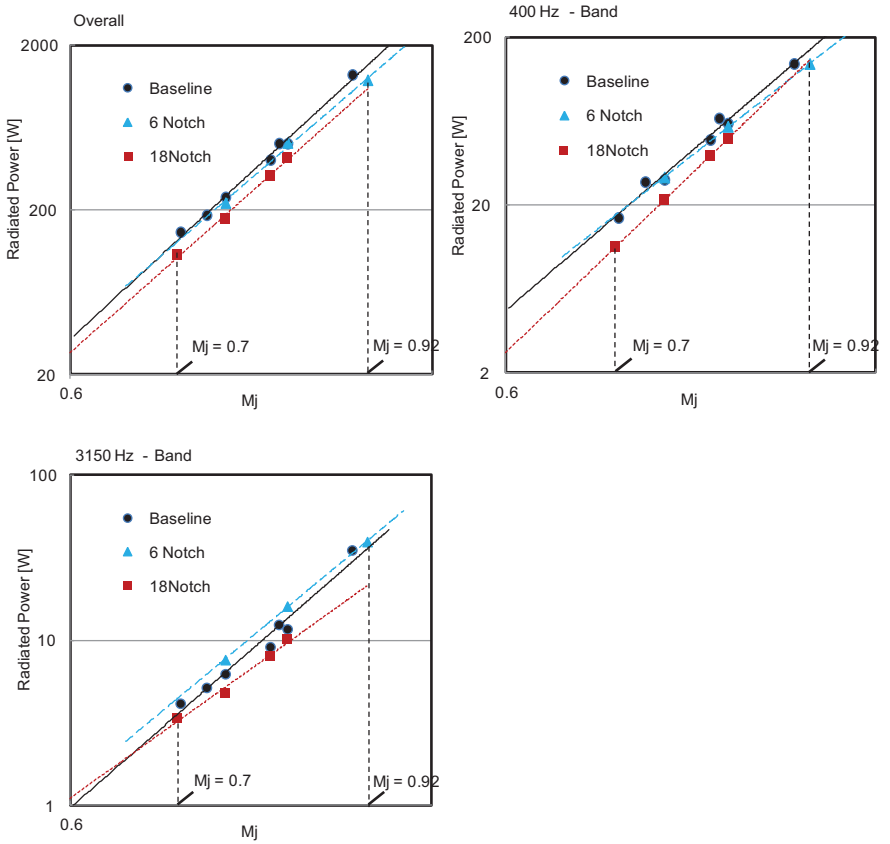

(2) Perceived noise level (PNL)

A simple estimation of the PNL [24] was carried out to evaluate the noise benefit of the 18-notched nozzle. This estimation dealt with only the jet mixing noise and did not consider any other noise such as the fan noise. The lateral attenuation during sound propagation from the aircraft to the observer was referred from a model in a technical manual [25]. The far-field noise data obtained in the engine test were input in the computation. The nozzle diameter was scaled up to 2.5 times that of the engine nozzle. The concerned 1/3 octave band frequency ranged from 50 Hz to 11,200 Hz bands in the PNL calculation. The

PNLs of the baseline nozzle and the 18-notched nozzle were compared at the flyover and lateral points, which are illustrated in Fig. 16. A rear-mounted twin-engine aircraft was assumed in this computation. The engine NPRs considered were 1.377, 1.436, and 1.536.

Fig. 16. Flyover (left) and lateral (right) points for the PNL estimation

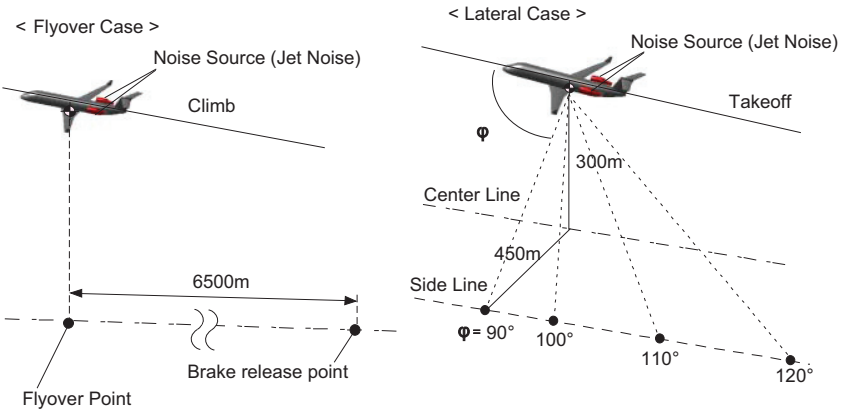

Figure 17 shows a plot of the noise margins from the baseline cases. The noise margin of the 18-notched nozzle is more than 1 dB greater at both the lateral and the flyover points.

(3) Future works

Some technical issues need to be overcome before the notched nozzle can be used in practice. With regard to the acoustic and aerodynamic performance, efforts should be continued to obtain additional acoustic and aerodynamic data that will help in improving the notch geometry. Additional experimental data should be obtained, and the measurement techniques used in the engine tests should be improved.

Fig. 17. Estimated noise margins of 18-notched nozzle relative to baseline nozzle at flyover and lateral points

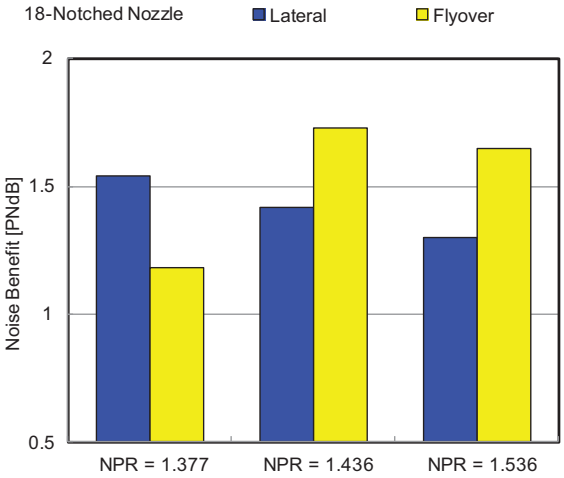

Concluding Remarks

The second engine noise test was carried out using a large-scale 18-notched nozzle with reduced notch depth and increased number of notches compared to previous 6-notched nozzles. The following observations were made in the noise test.

(1) The 18-notched nozzle well suppressed the jet mixing noise at a Strouhal number of around 0.25 without spillover of additional noise.

(2) The noise directivity confirmed the results of the hot-jet scale-model test, in that the 18-notched nozzle increased the noise margin toward the side direction.

(3) The radiated acoustic power, which well conforms to the power law, distinguished the effect of the 18-notched nozzle from that of the baseline nozzle.

(4) The source localization analysis clarified the jet noise source behind the nozzle and showed the noise reduction due to the notched nozzle.

(5) The 18-notched nozzle showed potential for noise reduction in terms of the PNL at both the lateral and the flyover positions.

Nomenclature

EGT	Exhaust Gas Temperature
I	Acoustic Power
NPR	Nozzle Pressure Ratio
PNL	Perceived Noise Level
P	Pressure
P_t	Total Pressure
M_j	Mach Number of Jet Flow
θ	Emission Angle from Jet Axis
κ	Specific Heat Ratio

Subscripts

6	Position after turbine
a	Standard State

Acknowledgments

The engine test was supported by JAXA's Noshiro Rocket Testing Center, IHI Corporation, INC Engineering Corporation, Bruel & Kjaer Japan, Science Service Inc., Tokyo University of Science, and JAXA's Jet Engine Technology Center. The authors would like to specially thank Mr. Hideshi Oinuma, Dr. Kenichiro Nagai, and Mr. Kei Wada for their technical support as well as Mr. Satoru Nakamura, Mr. Keishi Shintaku, and Ms. Yoshiko Shinoda for their help in analyzing the data and editing this paper.

References

[1] Smith, M. J. T., 1989, "Aircraft noise," *Cambridge University Press*.

[2] Gliebe, P. R., 1991, "Jet Noise Suppression, Aeroacoustics in Flight Vehicles: Theory and Practice," *NASA-RP-1258-Vol.2*.

[3] Casalinoa, D., et al., 2008, "Aircraft Noise Reduction Technologies: A Bibliographic Review," *Aerospace Science and Technology, Vol.12*.

[4] Oishi, T., et al., 2012, "Experimental and Computational Study on Jet Noise Reduction Devices Such as Notched, Chevron and Microjets," *ISUAAAT-JP12*.

[5] Martens, S., et al., 2011, "The Effect of Chevrons on Crackle Engine and Scale Model Results," *ASME Paper GT2011-46417*.

[6] Munday, D., Cuppoletti, D., et al., 2012, "Techniques for Supersonic Turbojet Noise Reduction," *ASME Paper GT2012-68304*.

[7] Tanaka, N., et al., 2012, "Jet Noise Reduction Using Microjet Configurations Experimental Characterization In CEPRA19 Anechoic Wind Tunnel," *AIAA-2012-2300*.

[8] Oishi, T., 2010, "Jet Noise Reduction by Notched Nozzle on Japanese ECO-Engine Project," *AIAA-2010-4026*.

[9] Ishii, T., et al., 2011, "Experimental Study on a Notched Nozzle for Jet Noise Reduction," *ASME Paper GT2011-46244*.

[10] Tanaka, N., et al., 2011, "Experimental and Computational Approach for Jet Noise Mitigation by Mixing Control Devices," *ASME Paper GT2011-45200*.

[11] Tanaka, N., et al., 2010, "The Effect of the Jet Noise Mitigation Using Large Eddy Simulation," *Proceedings of 38th GTSJ Conference (in Japanese), B21*.

[12] Ishii, T., et al., 2010, "Jet Noise Suppression by Mixing Control Devices," *Proceedings of 38th GTSJ Conference (in Japanese), B-22*.

[13] Ishii, T., et al., 2012, "Hot-jet Noise Test of a Revised Notched Nozzle," *ASME Paper GT2012-69507*.

[14] Tanaka, N., et al., 2012, "Thrust and Noise Estimation of a Jet Noise Reduction Device By the Pure Jet Engine Test," *Proceedings of 40th GTSJ Conference (in Japanese), B-20*.

[15] Zaman, K. B. M. Q., Bridges, J. E., and Huff, D. L., 2010, "Evolution from 'Tabs' to 'Chevron Technology' – a Review," *International Journal of Aeroacoustics, 10(5&6), pp. 685-710*.

[16] Zaman, K. B. M. Q., Reeder, M. F., and Samimy, M., 1994, "Control of an Axisymmetric using Vortex Generators," *Phys. Fluids, 6, pp. 778-793*.

[17] Ishii, T., et al., 2009, "The Outdoor Noise Test of a YJ69 Turbojet Engine," *JAXA-RM-08-012* (in Japanese).

[18] Tagashira, T., et al., 2011, "Application of Model-Based Control for JAXA's Engine Test," *IGTC-2011-0240*.

[19] SAE, 1990, "Measurement of Far Field Noise from Gas Turbine Engines During Static Operation," *ARP-1846*.

[20] Ishii, T., et al., 2012, "Experimental Study of a Claw Mixer," *AIAA Paper 2012-2301*.

[21] Hald, J., et al., 2012, "High-resolution Fly-over Beamforming Using a Small Practical Array," *AIAA Paper 2012-2229*.

[22] Flecher, J. S., and Smith, P. H., 1975, "The Noise Behavior of Aero Engine Turbine Tones," *AIAA Paper 1975-466*.

[23] Lighthill, M. J., 1952, "On Sound Generated Aerodynamically: 1. General Theory," *Proc. Roy. Soc. Lon. (A), 211, pp.564-587*.

[24] ICAO, 1995, "Environmental Technical Manual on the Use of Procedures in the Noise Certification of Aircraft," *Doc. 9501-AN/929*.

[25] SAE, 1981, "Prediction Method of Lateral Attenuation of Airplane Noise During Takeoff and Landing," *AIR-1751*.

Heat Conduction Correction in Reciprocity Calibration of Laboratory Standard Microphones*

Erling Sandermann Olsen†

Abstract

Primary pressure sensitivity calibration of laboratory standard microphones with the reciprocity technique is standardized in international standard, IEC Publication 61094-2:2009. The standard describes how to calculate the acoustical transfer impedance between pairs of microphones mounted in standardized couplers. However, the standard is open for interpretation on some points, and in particular two methods are given for calculation of corrections for heat conduction and viscous losses. The two methods are not consistent. The difference is significant as compared to other uncertainty components, and there is not a clear indication on how to choose between the methods. The choice of method may be based on consistency between couplers of different size, but the apparent consistency depends on the interpretation of other suggested calculations in the standard. In this paper, research is presented that indicates that the so-called low frequency domain solution is the most correct at low and medium frequencies. The low-frequency solution is an approximation to the so-called full frequency domain solution that must be used at very low frequencies. The calculation of the terminating impedances at the microphones is discussed. The losses and microphone impedances at high frequencies are also briefly discussed.

Résumé

La méthode primaire pour l'étalonnage en pression des microphones étalons de laboratoire par la méthode de réciprocité est décrite par la Publication CEI 61094-2:2009. Cette norme internationale décrit le mode de détermination de l’impédance acoustique de transfert entre deux microphones montés sur des

* First published at INTER-NOISE 2012, New York City, USA

† Brüel & Kjær Sound & Vibration Measurement A/S, Denmark

coupleurs normalisés. Or, la norme est sujette à interprétation sur certains points. En particulier, deux méthodes sont décrites concernant le calcul des corrections pour la conduction thermique et les pertes visqueuses. Ces deux méthodes ne sont pas en adéquation. Par rapport aux autres facteurs d'incertitude, la différence est significative, et aucune indication claire n'est fournie pour le choix de l'une ou l'autre méthode. Ce choix peut être basé sur la cohérence entre coupleurs de différentes tailles, mais l'adéquation apparente varie en fonction de l'interprétation des autres calculs suggérés par la norme. Ce document décrit des travaux qui montrent que la solution dite "low-frequency domain" est la solution plus correcte pour les fréquences basses et moyennes. Cette solution est une approximation dérivée de la solution dite "full frequency domain" qui doit être utilisée pour les très basses fréquences. Le calcul des impédances de terminaison des microphones est ici discuté, comme le sont aussi brièvement les pertes et les impédances microphoniques aux hautes fréquences.

Zusammenfassung

Die Primärkalibrierung des Druckübertragungsmaßes von Laboratoriums-Normalmikrofonen nach dem Reziprozitätsverfahren ist in der internationalen Norm IEC 61094-2:2009 standardisiert. Die Norm beschreibt, wie die akustische Übertragungsimpedanz zwischen Mikrofonpaaren berechnet wird, die in standardisierten Kupplern montiert sind. In einigen Punkten lässt die Norm jedoch Spielraum für Interpretation. Insbesondere werden zwei verschiedene Methoden zur Berechnung von Korrekturen für Wärmeleitungs- und viskose Verluste angegeben. Diese beiden Methoden sind nicht konsistent. Der Unterschied wird beim Vergleich mit anderen Unsicherheitskomponenten deutlich und es gibt keine klaren Hinweise für die Auswahl der Methode. Zur Wahl der Methode kann die Konsistenz zwischen Kupplern unterschiedlicher Größe herangezogen werden, jedoch hängt die scheinbare Konsistenz von der Interpretation anderer in der Norm vorgeschlagener Berechnungen ab. In diesem Artikel werden Forschungsergebnisse vorgestellt, die darauf hindeuten, dass die so genannte "low-frequency domain"-Lösung bei niedrigen und mittleren Frequenzen korrekter ist. Die Lösung für niedrige Frequenzen stellt eine Näherung für die so genannte "full frequency domain"-Lösung dar, die bei sehr niedrigen Frequenzen verwendet werden muss. Es wird die Berechnung der Abschlussimpedanzen an den Mikrofonen diskutiert. Die Verluste und Mikrofonimpedanzen bei hohen Frequenzen werden ebenfalls kurz diskutiert.

Introduction

As of today, the primary standard for sound pressure level is defined indirectly through the sensitivity of laboratory standard (LS) microphones. The capability of measuring sound pressure therefore depends on the uncertainty of measurement of the absolute sensitivity of LS microphones and of the methods used to transfer the sensitivity to sound measuring devices such as sound level meters and couplers used for audiometer and telephone measurements. In order to be able to calibrate sound measuring devices for use in different sound fields, it is necessary to know the pressure sensitivity as well as the free-field sensitivity of LS microphones. The subject of this paper is reciprocity calibration of pressure sensitivity of LS microphones, and in particular the calculation of the acoustic transfer impedance of the calibration couplers at low frequencies.

Primary pressure sensitivity calibration of laboratory standard microphones with the reciprocity technique is standardized in international standard, IEC Publication 61094-2:2009 [1], IEC 61094-2 for short. In IEC 61094-2 it is described how to calculate the acoustical transfer impedance between pairs of microphones mounted in standardized couplers. However, the standard is open for interpretation on some points, and in particular two methods are given for calculation of corrections for heat conduction and viscous losses, and the two methods are not consistent. The choice of method may be based on consistency between couplers of different size, but the apparent consistency depends on the interpretation of other suggested calculations in the standard.

For measurement of pressure sensitivity of LS1 microphones with today's measurement techniques, the uncertainty of measurement due to reproducibility, electrical and mechanical quantities, static pressure and temperature corrections etc., can be less than 0.015 dB at frequencies from around 3 kHz down to 2 Hz [2]. However, this uncertainty is valid under the assumption that the theory behind the calculations is correct.

In this paper the calculation of the losses due to heat conduction and viscosity at low frequencies and the calculation of the terminating impedances at the microphones are discussed The losses and microphone impedances at high frequencies are also briefly discussed.

Calculations and Results

Heat Conduction Correction

The transfer impedance of the coupler with the microphones can only be calculated assuming a loss-free, purely adiabatic sound field in a limited frequency range and with limited accuracy. Heat conduction and viscous losses near the surfaces in the coupler will influence the transfer impedance. Annex A of IEC 61094-2 [1] presents two methods for the calculation of corrections for losses due to heat conduction and viscous losses, referred to in the standard as the low-frequency solution and the broadband solution.

The low-frequency solution is based on Gerber's paper [3] with Gerber's solution for a rigid piston driver [4], equation (33) of the paper. The low-frequency solution is derived under the assumptions of the same instantaneous pressure in the entire coupler and that losses due to viscosity and convection are negligible. It is mentioned in clause A.2 in IEC 61094-2 that the so-called full frequency domain solution given by Gerber must be used at very low frequencies, whereas his short-term solution given in expression (A.2) in the annex is only valid at frequencies above 25 Hz for LS1 microphones in plane wave couplers ($X > 5$ in IEC 61094-2). This does not, however, constitute a practical limitation, as only rather few terms are needed for the calculation of the full frequency domain solution for frequencies where expression (A.2) is not sufficiently accurate. The two formulations can therefore be combined for efficient calculation. Note that in the following this combined approach is used when the low-frequency solution is referred to.

The broadband solution is based on the theory derived for sound propagation in a cylindrical tube, which again is based on the theory of Kirchhoff [1,4 – 7]. In this solution the viscous and thermal losses are accounted for by a complex propagation coefficient and a complex characteristic impedance of the tube based on simplifying assumptions for the analytical solution [7], and the losses at the ends of the tube are accounted for by calculation of the thermal boundary layer impedance.

The difference between results calculated with the broadband solution and the low-frequency solution are shown in Fig. 1.

Two important observations can be made from Fig. 1. The first is that at frequencies up to around 50 Hz, the two solutions differ substantially more than the uncertainty that can be considered achievable for reciprocity calibrations as mentioned above [2]. The difference is actually large enough to be comparable to

Fig. 1. Difference between corrections for losses calculated with the low-frequency solution and the broadband solution. The difference is shown for four 18.6 mm couplers of different length

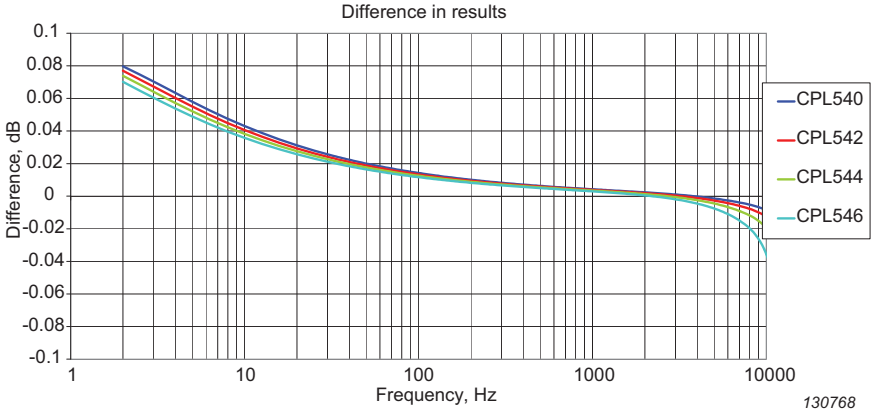

any other uncertainty component up to around 1 kHz. This means that both methods cannot be valid at low frequencies, although the text in the standard indicates so. The other observation is that there is no immediately reasonable way to combine the two methods. The difference does cross zero at a certain frequency, but with a slope significantly different from zero. This means that there is no 'transition' range where both solutions can be assumed to be valid.

A third observation can be made from the expressions in Gerber's paper and IEC 61094-2. The low-frequency limit of the broadband solution is similar to the short-term solution for a zero impedance driver. As the frequency approaches zero, the results calculated with the broadband solution approach infinity, evidently in contradiction with the fact that at sufficiently low frequencies isothermal conditions prevail in the coupler and the (sound) pressure is inversely proportional to the volume of the coupler, whereas the (full) low-frequency solution correctly approaches the ratio of specific heats. Thus, for very low frequencies, the broadband solution is clearly too simple and leads to incorrect results.

Impedances at the Microphones

The acoustic impedances of the microphone diaphragms are parts of the transfer impedance of the coupler with the microphones, cf. equations (3) and (4) of IEC 61094-2 [1]. It is recommended in the standard to express the impedance of

each microphone in terms of an equivalent series connection of compliance, mass and resistance. It is stated that the model is valid at frequencies up to 1.3 times the resonance frequency of the microphone and that a wrong equivalent volume mainly influences the calculated sensitivity at frequencies above the resonance frequency, although it is mentioned that the model is only a first approximation to the microphone impedance and that the equivalent volume increases towards low frequencies due to changes in the acoustic impedance of the back cavity in the microphone. To the knowledge of the author, the simple model has hitherto been the only model used in the context of calculation of the transfer impedance of couplers in reciprocity calibrations, although more complicated models have been suggested, for example, for modelling the static pressure dependence of LS microphones [8].

At low frequencies the open-circuit pressure sensitivity of an LS microphone is proportional to the admittance of the diaphragm, as the unloaded output is proportional to the volume displacement of the diaphragm and it is reasonable to assume that the pressure is uniform over the diaphragm due to the wavelengths. Therefore, the relative change in the microphone impedance can be derived from the pressure sensitivity. The typical low-frequency behaviour of the pressure sensitivity of an LS1 microphone is shown in Fig. 2. The sensitivity at 1 Hz is around 1.4 dB, or 17%, higher than the minimum value. Assuming an equivalent volume of 135 mm^3 at frequencies where adiabatic conditions can be assumed to exist in the back cavity of the microphone, this corresponds to an increase of

Fig. 2. Typical relative low-frequency pressure sensitivity of an LS1 microphone

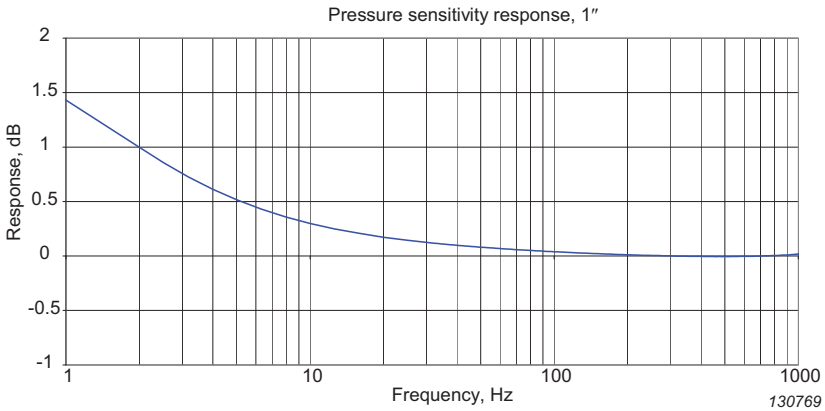

around 23 mm^3. Theoretical values for a typical LS1 microphone based on a static pressure coefficient of −0.016 dB/kPa are 7.5 mm^3 due to isothermal behaviour and 30 mm^3 when vent is fully open (0 Hz). For comparison, a variation of the total volume (sum of front cavity and equivalent volumes) of 3 mm^3 can clearly be seen in the calibration result.

Some microphones have additional surface area in the cavity. Additional surface area may be due to the thread in the front cavity ring in some (old) LS1 microphones or to the ring volume in working standard (WS) microphones with a cavity ring mounted for reciprocity calibration. This additional surface may contribute to the heat conduction losses as suggested by Frederiksen [9]. However, the dimensions of the thread and the width of the ring volume may be comparable to the thickness of the thermal boundary layer at frequencies where the heat conduction is of significant influence. Hence, the heat conduction correction due to additional surface in the cavity may be overestimated, if the surface area is included as suggested in IEC 61094-2.

Above the resonance frequency, the sensitivity of LS microphones decreases with frequency at a higher rate than expected from the simple microphone impedance model. This makes a unique determination of the three parameters difficult and suggests that the model is too simple, even around the resonance frequency. Although it is beyond the scope of this paper, it is mentioned here because it may have influence on the considerations concerning the loss model. Therefore, a thorough analysis will probably be useful in the search for a loss model that is consistent in the full frequency range of calibrations.

Numerical Calculation

In order to provide a third approach for comparison with the low-frequency solution and the broadband solution discussed here, a simple model has been implemented in COMSOL Multiphysics® [10]. In the model two simple diaphragms are placed, one in each end of a cylindrical coupler, and the system is excited by applying a uniform force to the outside of one of the diaphragms. The calculations were made assuming a sound field with thermal and viscous losses due to the walls and repeated assuming adiabatic conditions in the coupler. The difference between the results is shown in Fig. 3. The heat conduction correction calculated with the low-frequency solution for the same configuration is also shown in Fig. 3. The numerical calculation seems to be consistent with the low-frequency solution at very low frequencies, but at frequencies above a few hertz it indicates that the sensitivity may be underestimated with both solutions in IEC 61094-2. This observation was not investigated further at the time of writing.

Fig. 3. Comparison of correction for losses calculated with a) numerical method, b) low-frequency solution, c) broadband solution (low-frequency approximation)

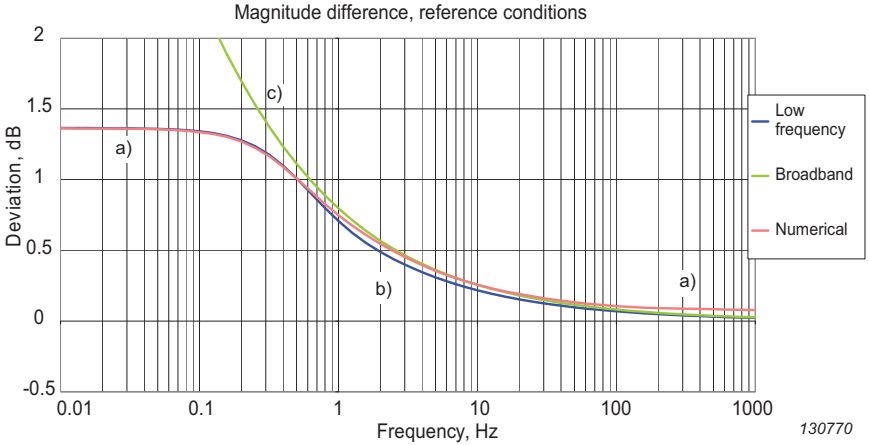

Measurements in Different Couplers

As the sensitivity of the microphone shall be independent of the coupler used, a way to determine the microphone parameters and at the same time to verify consistency in measurements is to measure with more than one coupler. The microphone parameters can then be adjusted so that the same calibration result is achieved in the four couplers. This is the data-fitting method referred to in E.3 and E.4 of IEC 61094-2. However, as also noted in IEC 61094-2, the appropriate corrections must be applied in order to achieve the correct result. Heat conduction, viscous losses, radial wave motion and the terminating impedance at the ends of the couplers all have influence on the results and must be calculated correctly. Not applying all corrections correctly may lead to wrong conclusions.

In Fig. 4 the deviations from the mean results of measurements in four different couplers are shown for four different calculation scenarios. The results shown are for an LS1 microphone with no thread in the front cavity ring. The calculations were made with the broadband solution and the low-frequency solution, in each case with and without taking into account the increase in microphone compliance towards low frequencies. For each scenario the front cavity volume and equivalent diaphragm volume (V_{eq}) were adjusted so as to minimize the difference between the results from the four couplers. In Fig. 5 the differences between the results of the four scenarios are shown.

Fig. 4. Variation with coupler for a) broadband solution, fixed V_{eq}, b) broadband solution, V_{eq} frequency dependent, c) low-frequency solution, fixed V_{eq}, d) low-frequency solution, V_{eq} frequency dependent

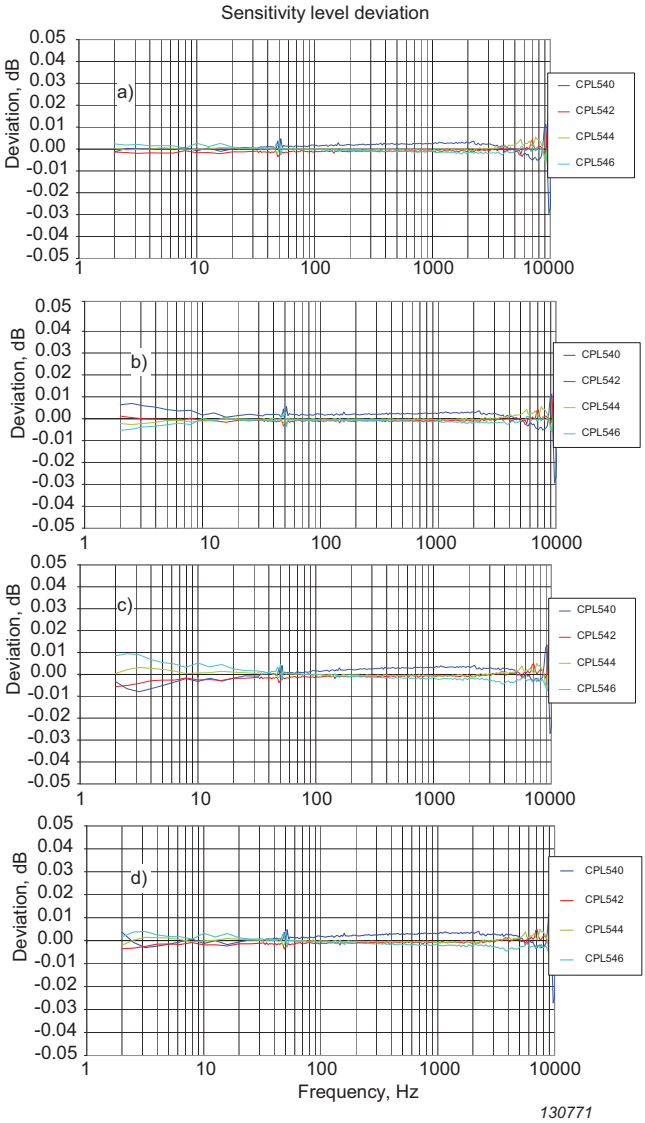

Fig. 5. Variation of results with a) broadband solution, fixed V_{eq}, b) broadband solution, V_{eq} frequency dependent, c) low-frequency solution, fixed V_{eq}, d) low-frequency solution, V_{eq} frequency dependent

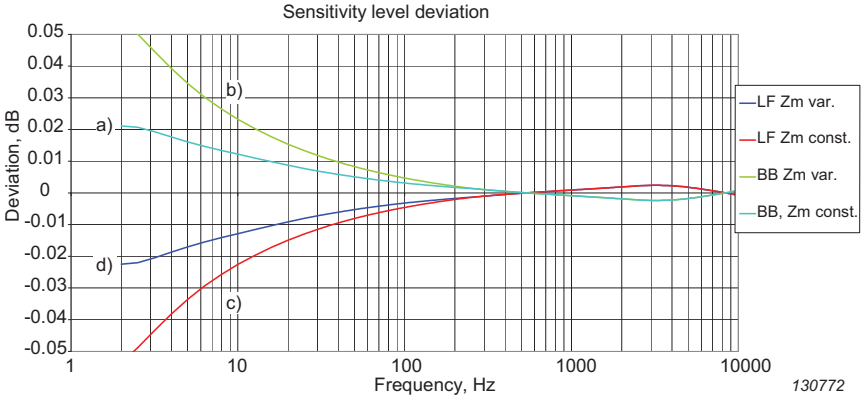

As can be seen from Fig. 4 and Fig. 5, it is possible to repeat measurements in different couplers with variation substantially less than 0.01 dB from 2 Hz to 1 kHz, but the differences between the results from the different calculation scenarios are large as compared to all other uncertainty components. It is noted that at frequencies above 20 Hz there does not seem to be any systematic difference in the variations between the scenarios. At lower frequencies there are, however, differences, although they are subtle. Assuming frequency-independent diaphragm impedance, the broadband solution appears to be very consistent, but when the low-frequency variation of the diaphragm impedance is included in the calculations, differences between the results appears below 20 Hz. The opposite happens with the low-frequency solution. Here the results are consistent when the frequency variation of the diaphragm impedance is included.

In Fig. 6 the deviations from the mean results of measurements in four different couplers are shown for an LS1 microphone with a thread in the front cavity ring. The calculations were made with the low-frequency solution taking the increase in microphone compliance towards low frequencies into account. In the three calculations the additional surface area due to the thread was added fully to the surface area, not added to the surface area, and added partly to the surface area of the coupler. The differences between the results of the three calculations are shown in Fig. 7. As can be seen from the figures, fully including the surface area of the thread in the calculations seems to lead to overcompensation at very low

frequencies. On the other hand, not including the additional surface area at all seems to make it difficult to achieve optimal consistency between the couplers.

Fig. 6. Variation with coupler for microphone with thread in front cavity. a) additional surface fully included, b) additional surface partly included, c) additional surface not included

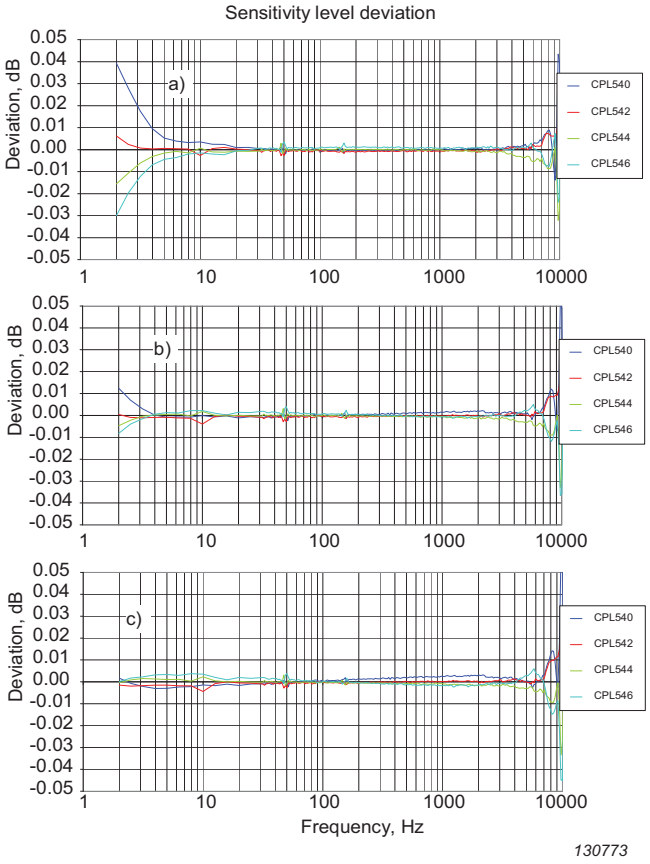

Discussion

As reciprocity calibration based on IEC 61094-2 constitutes the present primary sound level standard, the reliability of these calibrations in terms of the uncertainty of measurement is of high importance in all contexts where sound level is

Fig. 7. Variation of results for microphone with thread in front cavity. a) additional surface fully included, b) additional surface partly included, c) additional surface not included

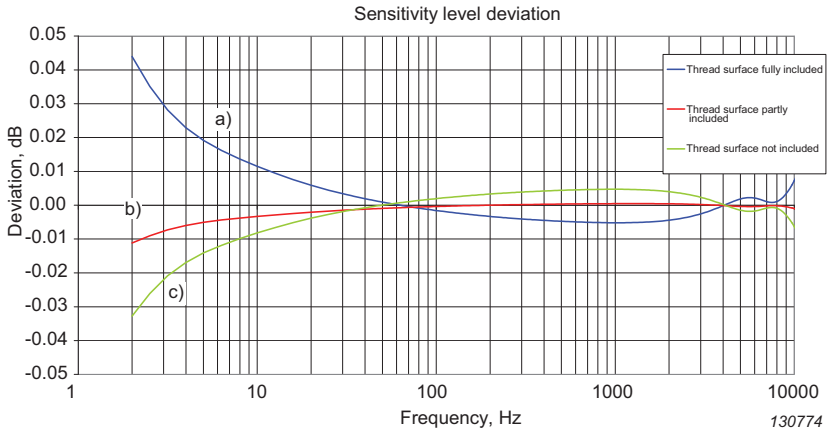

measured. The methods of the standard should, therefore, continuously be subject to critical review. Furthermore, as the frequency range of reciprocity calibration has been extended towards lower frequencies in recent years, it is relevant to revise the method with respect to uncertainty at low frequencies.

As shown in the previous sections, the two approaches of IEC 61094-2 for determining the transfer impedance of couplers taking into account thermal losses are not consistent, and the standard does not give clear indications on how to choose between the approaches. For the broadband solution it is stated that it is valid above 3 Hz for LS1 microphones, but no estimate of uncertainty is given. The low-frequency solution is stated to be accurate to 0.01%, or 0.001 dB, at frequencies above 25 Hz for LS1 microphones in plane wave couplers ($X > 5$), but no upper frequency limit for that accuracy is given. Even at 50 Hz, the difference between the two solutions is around 0.02 dB, more than an order of magnitude larger the 0.01% and larger than any other uncertainty component in the calibration, and certainly also large enough to have influence on the uncertainty of measurement in calibration of sound calibrators that is normally considered to be 0.1 dB or better [11]. As long as there are no clear evidence what the correct approach for calculation of the transfer impedance is, the difference must be accounted for in the estimation of the uncertainty of measurement. Thus, there is clearly a need to resolve the ambiguity.

The results presented here indicate that the low-frequency solution is the better model of the two for the calculation of the coupler transfer impedance at frequencies where spatial variation of the pressure in the coupler can be ignored. The zero-frequency limit of the solution corresponds to purely isothermal conditions in the coupler, it provides consistency between different couplers at frequencies below 20 Hz when the microphone impedances are calculated correctly, and it is reasonably consistent with numerical modelling at very low frequencies. The results do not, however, clearly indicate the upper frequency of validity of the low-frequency solution or how close the solution is to the physically correct result.

The results show that the variation with frequency of the microphone impedances at low frequencies must be taken into account in the calculations. If it is not taken into account, wrong conclusions may be drawn from measurements in multiple couplers. The interaction between the microphone impedances and the heat conduction model was shown. Similar interaction can be shown for the influence of additional surface area. The relative impedance variation of LS2 microphones is much smaller than that of LS1 microphones, but as it is fundamentally more correct to include it in the calculations it should always be done.

The influence of the thread in the front cavity of some older LS1 microphones needs further investigation. This is of importance, as long-term sensitivity history is essential for the continuous validation of primary microphone calibrations and many established references are still LS1 microphones with the thread. The results presented here indicate that the increase in coupler surface area due to the thread has to be taken partly into account.

The results shown and the discussion here are only based on the sensitivity level, whereas the phase should evidently also be measured and the transfer impedance phase calculated correctly. However, the differences and the apparent consistencies and inconsistencies of the different calculations are clearly illustrated with the differences in the sensitivity level and therefore only the level has been discussed here.

There is clearly a need for revision of the theory for calculation of the sound field in couplers for reciprocity calibration and thereby the acoustic transfer impedance of the couplers. The theory must be consistent in the full frequency range of the calibration.

As shown, it is possible to make measurements in different couplers with high consistency, and as mentioned in the introduction the uncertainty of measurement

can be less the 0.015 dB at low and medium frequencies, given a correct theory for the measurements. This is encouraging as it indicates that an uncertainty of measurement of that order of magnitude is within reach.

Conclusions

In this paper the calculation of the acoustic transfer impedance in couplers for reciprocity calibration of pressure sensitivity of LS microphones at low frequencies has been discussed. The following can be concluded:

- Two methods for calculating the transfer impedance are described in international standard IEC 61094-2:2009. The methods do not give consistent results at any frequency
- The results presented here indicates that the low-frequency solution gives results closest to the real physics at low frequencies, but further research is required to determine the accuracy and the upper frequency limit of the solution
- The broadband solution may be the right solution at high frequencies, but there is no simple transition between the two solutions
- The low-frequency variations in the microphone impedances must be included in the calculation of the transfer impedance in order to give consistent results
- The influence of additional surface due to a thread in the front cavity ring cannot be accounted for by simply adding the additional surface area in the expressions. This influence requires further investigation. Until the loss models have been revised and the revised models have found their way into standardization, the ambiguity of the transfer impedance calculation must be accounted for in the uncertainty of measurement

Acknowledgements

The author gratefully acknowledges Knud Rasmussen and Salvador Barrera-Figueroa at Danish Fundamental Metrology and Richard Jackett at National Physical Laboratory, UK for valuable and critical discussions on the subject of this paper. The author also gratefully acknowledges Brüel & Kjær Sound & Vibration

Measurement A/S for recognizing the importance of the work with primary calibration.

References

[1] IEC 61094-2:2009, Measurement microphones – Part 2: Primary method for pressure calibration of laboratory standard microphones by the reciprocity technique.

[2] Uncertainty calculations by the author for implementation of the methods of reference 1 in BKSV-DPLA.

[3] H. Gerber, "Acoustic properties of fluid-filled chambers at infrasonic frequencies in the absence of convection", *J. Acoust. Soc. of Am*., **36**. (1964).

[4] K. Rasmussen, "On the calculation of heat conduction in cylindrical cavities", *Internal Report PL-02, Denmark 1990*.

[5] C. Zwikker and C.W. Kosten, "Sound Absorbing Materials", *Elsevier, Amsterdam*, 1949 (reference [A.2] of reference 1.).

[6] P.M. Morse and K.U. Ingard, "Theoretical Acoustics", *McGraw-Hill, New York, 1968* (reference [A.3] of reference 1.).

[7] C. Guianvarc'h, J.-N. Durocher, M. Bruneau and A.-M. Bruneau, "Acoustic transfer admittance of cylindrical cavities", *J. Sound and Vib., 292 (2006)*.

[8] K. Rasmussen, "The static pressure and temperature coefficients of laboratory standard microphones", *Metrologia, 36 (1999)*.

[9] E. Frederiksen, "Reduction of Heat Conduction Error in Microphone Pressure Reciprocity Calibration", *Brüel & Kjær Technical Review No. 1, 2010*.

[10] COMSOL Multiphysics version 4.2. Finite element modelling software by COMSOL, 2011.

[11] The BIPM Key Comparison Database, BIPM-KCDB. CMC values for pistonphones.

Previously issued numbers of Brüel & Kjær Technical Review

(Continued from cover page 2)

1 – 2001 The Influence of Environmental Conditions on the Pressure Sensitivity of Measurement Microphones
Reduction of Heat Conduction Error in Microphone Pressure Reciprocity Calibration
Frequency Response for Measurement Microphones – a Question of Confidence
Measurement of Microphone Random-incidence and Pressure-field Responses and Determination of their Uncertainties
1 – 2000 Non-stationary STSF
1 – 1999 Characteristics of the vold-Kalman Order Tracking Filter
1 – 1998 Danish Primary Laboratory of Acoustics (DPLA) as Part of the National Metrology Organisation
Pressure Reciprocity Calibration – Instrumentation, Results and Uncertainty
MP.EXE, a Calculation Program for Pressure Reciprocity Calibration of Microphones
1 – 1997 A New Design Principle for Triaxial Piezoelectric Accelerometers
A Simple QC Test for Knock Sensors
Torsional Operational Deflection Shapes (TODS) Measurements
2 – 1996 Non-stationary Signal Analysis using Wavelet Transform, Short-time Fourier Transform and Wigner-Ville Distribution
1 – 1996 Calibration Uncertainties & Distortion of Microphones.
Wide Band Intensity Probe. Accelerometer Mounted Resonance Test
2 – 1995 Order Tracking Analysis
1 – 1995 Use of Spatial Transformation of Sound Fields (STSF) Techniques in the Automative Industry

Special technical literature

Brüel & Kjær publishes a variety of technical literature that can be obtained from your local Brüel & Kjær representative.

The following literature is presently available:

- Catalogues
- Product Data Sheets

Furthermore, back copies of the Technical Review can be supplied as listed above. Older issues may be obtained provided they are still in stock.

www.bksv.com

BV 0065 – 11 ISSN 0007 – 2621

HEADQUARTERS: Brüel & Kjær Sound & Vibration Measurement A/S
DK-2850 Nærum Denmark · Telephone: +45 7741 2000 · Fax: +45 4580 1405
www.bksv.com · info@bksv.com

Brüel & Kjær

Local representatives and service organisations worldwide